CRYSTAL CHEMISTRY AND DIFFERENTIAL THERMAL EFFECTS OF DOLOMITE*†

W. F. BRADLEY,[1] J. F. BURST,[2] AND D. L. GRAF.[3]

ABSTRACT

It is observed that the lower temperature endothermal effect of dolomite takes place at a considerably lowered temperature after the dolomite has been subjected to prolonged vigorous grinding.

The mechanisms and consequences of plastic deformation in the dolomite crystallization are discussed, and are contrasted with the analogous deformations in the simple carbonates. Multiply deformed dolomite crystals actually contain island nuclei locally enriched in one or the other of the positive ions. Powder diffraction diagrams of such deformed crystallites exhibit greatly attenuated intensities for those reflections for which the form factor includes the term Ca-Mg.

An approximate evaluation of the four variable parameters of dolomite (in $R\bar{3}$) has been made, based on the powder diffraction. 2 C are in 2(c) with $x_0=0.243$ and 6 O are in 6(f) with $x_0=0.500$, $y_0=-0.042$ and $z_0=0.271$.

Among the abnormal differential thermal features exhibited by many dolomites, it has become apparent that some, at least, may be consequences of structural factors. An attempt has been made through extended grinding to alter mechanically the structural arrangement of a dolomite lattice and to record this alteration through variations of the differential thermal pattern and the *x*-ray diffraction effects.

The nature of the material resulting from this type of mechanical stressing precludes single crystal work, making the use of powders necessary for both *x*-ray diffraction and thermal analysis. It is thus desirable to establish with moderate accuracy the variable carbon and oxygen parameters. By drawing heavily on the crystal chemistry data available for the various simple rhombohedral carbonates, a suitable model is readily established from which refinements can be made.

The dolomite structure consists of hexagonally packed layers of carbonate groups between which alternate layers of octahedral interstices are occupied respectively by calcium and magnesium. A trial model is obtained by combining one layer of $CaCO_3$ from calcite with one layer of $MgCO_3$ from magnesite in such a manner that each layer assumes the dolomite translation, and the carbonate groups of each become coincident. This operation moves the carbonate groups toward the magnesium

* Published with permission of the Chief, Illinois State Geological Survey, and of the Shell Oil Co.

† This contribution is condensed from material originally planned as separate publications by the respective laboratories.

[1] *X*-Ray Division, Illinois State Geological Survey, Urbana, Illinois.

[2] Exploration and Production Research Division, Shell Oil Company, Houston, Texas.

[3] Industrial Minerals Division, Illinois State Geological Survey, Urbana, Illinois.

layers and maintains one of the carbonate oxygens in each of the three cleavage planes.

The simple rhombohedral carbonates crystallize in $R\bar{3}c$ and dolomite in $R\bar{3}$; the lattice translations are all accurately known (Bragg) (1). The best established C—O bond length is the 1.31 Å value deduced by Elliott (3). Using this value, the Ca—O bond in calcite is 2.34 Å, and the Mg—O bond in magnesite is 2.06 Å.

When set up so that planar CO_3 groups of C—O bond 1.31 Å are oriented with one oxygen in each cleavage plane, the structure is effectively reduced to the one variable parameter x_c. Best agreement between observed and calculated powder diffraction intensities is near $x_c = 0.243$. Agreement deteriorates noticeably at x_c deviations of $\pm .003$. At $x_c = 0.243$ the Ca—O and Mg—O bonds are respectively 2.34 and 2.08 Å. In Table 1, spectrometer counts from a G.E. recording spectrometer reduced according to the formula:

$$q\alpha \frac{1 + \cos^2 2\theta}{\sin^3 \theta \cos \theta} pF^2$$

and, approximately scaled to absolute F's, are compared with calculated form factors for Ca at 0, 0, 0; Mg at $\frac{1}{2}, \frac{1}{2}, \frac{1}{2}$; 2C at $\pm x_c = 0.243$; and 6O in 6(f) at $x_0 = 0.500$, $y_0 = -0.042$, $z_0 = 0.271$, etc. The factor

$$\frac{1}{\sin \theta}$$

is introduced as an arbitrary correction for focusing conditions.

The atomic scattering factors employed are those of Pauling and Sherman (8). Some improvement in agreement for the first few lines would be realized by allowance for the partial ionic character of the Me—O bonds. Further refinement of parameters would require recourse to higher angle diffraction and single crystal methods, which would differentiate reflections to which the oxygen contributions are of two kinds.

The quality of agreement of the data in Table 1 establishes that the above-described model is an adequate basis on which to discuss the mechanical processes described below.

The effects of grinding field-samples of dolomite were investigated as a function of time by placing them in an electric-powered mortar and pestle from which samples of the material being ground were withdrawn at various intervals for differential thermal analysis and x-ray diffraction analysis. It was soon noted that prolonged grinding produced definite abnormalities in the physical characteristics of the materials. Therefore, the experiments were duplicated with U. S. B. S. Dolomite No. 88 in an attempt to assign the abnormalities directly to the dolomite structure rather than to some unknown condition within the field sample. The

TABLE 1. COMPARISON OF CALCULATED AND OBSERVED RELATIVE F VALUES FOR POWDER DIFFRACTION LINES UP TO $2\theta = 70°$

Index	sin θ	Form Factor			F Calc.		Reduced from Spectrometer Count
100	.1243	Ca−Mg	+0.09 C	−0.33 O	+ 4.3		2.8
110	.1357	Ca+Mg	−1.99 C	−1.41 O	+ 7.4		5.0
112	.1736	Ca+Mg	+1.97 C	+1.49 O	+41.7		49
222	.1878	Ca+Mg	−1.93 C	−5.79 O	−18.4		20.0
221	.1974	Ca−Mg	+0.43 C	+0.70 O	+10.7		11.5
$1\bar{1}0$	.2084	Ca+Mg	+2 C	−2.44 O	+15.3		12.5
210, 120	.2286	Ca−Mg	−0.26 C	+4.63 O	+28.0	23	19
				−4.00 O	−17.3		
$11\bar{1}$	.2427	Ca−Mg	+0.09 C	+1.27 O	+11.1		11.3
200	.2486	Ca+Mg	−1.99 C	+1.80 O	+23.8		24.5
322	.2499	Ca−Mg	−0.60 C	−0.06 O	+ 2.2		2
220	.2713	Ca+Mg	+1.97 C	−2.13 O	+15.5		14
332	.2778	Ca+Mg	+1.86 C	+1.23 O	+29.7		40*
123, 213	.2806	Ca+Mg	−1.93 C	+3.48 O	+29.6	24	30*
				+1.23 O	+19.9		
333	.2815	Ca−Mg	+0.80 C	+2.40 O	+16.4		
311	.2870	Ca−Mg	+0.43 C	−1.74 O	− 2.5		no certain count
$2\bar{1}0$, $1\bar{2}0$	.3199	Ca−Mg	+0.09 C	+3.10 O	+15.4	13	12
				−3.71 O	−10.5		
$1\bar{1}2$, $\bar{1}12$	.3245	Ca+Mg	−1.99 C	+0.20 O	+14	19	17
				+2.46 O	+22.6		
334	.3353	Ca+Mg	−1.80 C	−1.48 O	+ 8.3		11
130, 310	.3420	Ca+Mg	+1.97 C	−1.48 O	+15.9	17	17
				−0.90 O	+18.0		
224	.3472	Ca+Mg	+1.86 C	−1.35 O	+16.2		21*
234, 324	.3504	Ca−Mg	+0.80 C	+3.08 O	+15.5	14	16*
				−4.95 O	−12.5		
230, 320	.3546	Ca−Mg	+0.43 C	+3.08 O	+14.7	11	12
				−2.70 O	− 5.4		
$11\bar{2}$	.3610	Ca+Mg	+2 C	+3.21 O	+31.5		26
300	.3730	Ca−Mg	−0.26 C	+0.18 O	+ 3.1		
$22\bar{1}$	.3731	Ca−Mg	−0.26 C	−1.02 O	− .8		36
444	.3754	Ca+Mg	+1.73 C	+5.19 O	+37.8		

Entries marked (*) include some spurious count from incompletely resolved adjacent strong lines.

same striking results, obtained with the field sample, were duplicated precisely through the grinding of the standard material.

After continuous grinding for a period of eight hours, dolomite was noted by differential thermal analysis to undergo an additional, small

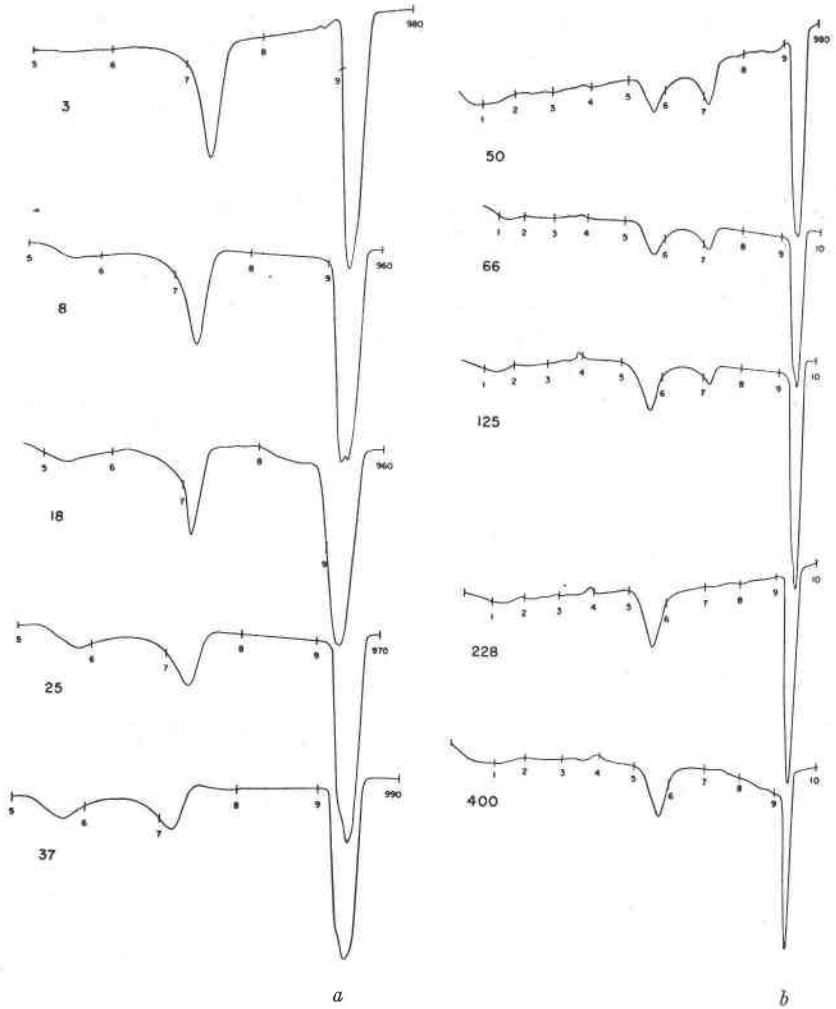

FIG. 1. Differential thermal analysis curves of U. S. B. S. Dolomite No. 88. Index numbers denote the times of grinding.

endothermic reaction between 500° and 600° C. This endothermic reaction is shown in curve 8, figure 1*a*. Curves on this plate show changes resulting from grinding, as recorded by differential thermal analysis. By employing Rowland and Lewis' (9) technique of furnace-atmosphere control, the carbonate peaks are separated and the area of each loop easily discernible. Curves in figure 1*a* show the thermal expressions from 500° to 1000° C. for material ground 3, 8, 18, 25, and 37 hours, respectively. Curves in figure 1*b* show thermal expressions for the entire range,

or room temperature to 1000° C., for material ground 50, 66, 125, 228, and 400 hours, respectively. The chart speed was decreased after the sample ground for 37 hours was analyzed because it had become apparent that a new endothermic loop was being formed which would be more suitably represented in a recording made at a slower chart speed.

The continued grinding increases the magnitude of the 500°–600° C. endothermic reaction at the expense of the 700°–800° C. endothermic reaction, commonly spoken of as the evolution of CO_2 from the $MgCO_3$ portion of the dolomite composition. This reciprocal variation is illustrated by the nested curves in figure 1. Also, it was found that the ratio of the sum of the areas of the two low-temperature peaks to the area of the high-temperature peak was virtually identical in each record. Several interesting relationships between the areas of the various loops are presented in figure 2.

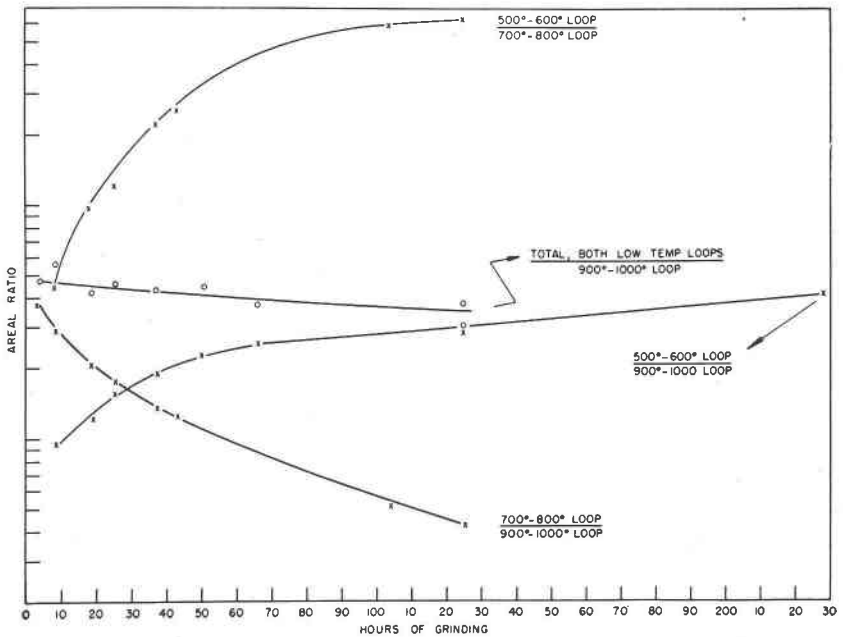

FIG. 2. Areal relationships of the three separate endothermal *DTA* features of various ground dolomite specimens.

It should be noted that the newly formed loop (figure 1) is considerably removed along the temperature axis from its progenitor and is, in this respect, unlike thermal anomalies which arise from particle-size diminution alone. When particle size is the controlling factor, a gradual lowering of the decomposition temperature usually is noted with decreas-

ing particle size. Interest is also aroused by the fact that after the 500°–600° C. loop is fully developed and the 700°–800° C. loop completely eliminated (228-hour grind), no further significant change is recorded even after prolonged grinding (400 hours).

X-ray powder diffraction diagrams of three ground samples, irradiated and recorded simultaneously under the strictest comparable conditions, show at least three lines which are selectively reduced in intensity upon continued grinding. These lines are recorded at $d=4.02$ Å, $d=2.53$ Å, and $d=2.06$ Å, and represent, respectively, the crystal planes (100), (221), and $(1\bar{1}1)$.

From Table 1 it can be noted that each of these planes ($h+k+l=$ odd) is characterized by a form factor of the type Ca minus Mg, modified by small to moderate carbon and oxygen contributions. The line-intensity diminutions are thought therefore to result from some specific structural alteration such as a glide mechanism whereby Ca^{++} and Mg^{++} ions would be migrated along certain directions within the lattice. When sufficient Ca^{++} ions have been translated to positions formerly occupied by Mg^{++} ions, so that a random distribution of these two ions is produced in the projection of the whole structure onto the poles to the planes in question, the lines representing those planes should almost disappear.

Examination of figure 3 indicates that reflections from planes (100), (221), and $(1\bar{1}1)$, which were relatively intense after three hours of grinding, became selectively less intense after 50 hours of grinding and virtually disappeared after 228 hours of grinding. It was at this point that the *DTA* curves also became stabilized (figure 1). The fact that these two circumstances prevail concurrently indicates the attainment of a new equilibrium established through the continued application of the nondirectional stress load. Crystallographic studies of plastic deformation in ionic crystals have been concerned primarily with directed loads as exemplified by Buerger's (2) analyses of the NaCl type face-centered cubes. There is no reason to assume that the translations so induced are the only ones which occur, and indeed, Buerger infers that deformations along octahedral planes are probably induced by random loading. Deformation along octahedral planes is also a frequent inference in diffraction analyses of orientation effects produced in the working of face-centered cubic metals.

The close structural analogy between the face-centered cubic alkali halides and the rhombohedral carbonates suggests that such structural consequences of deformations as could have resulted from the above grinding experiments could profitably be examined.

In order to avoid the confusion which arises from the various sets of reference axes to which rhombohedral carbonates are at times referred,

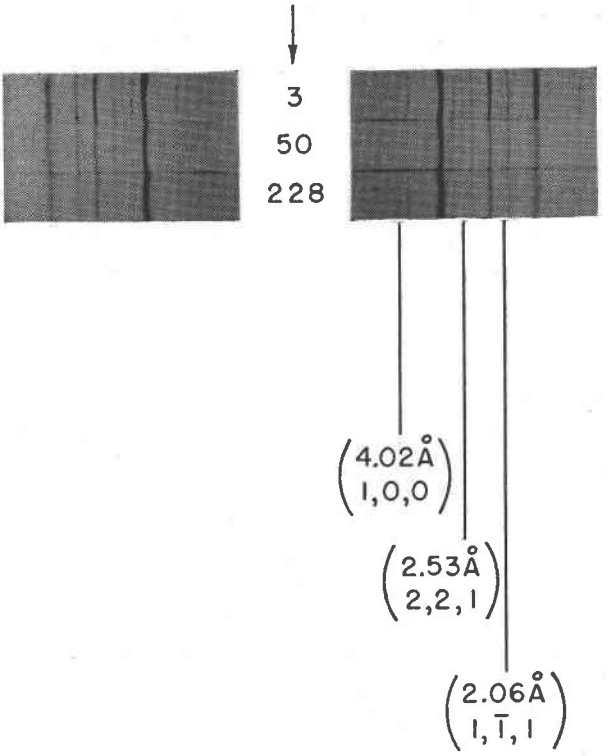

FIG. 3. Simultaneously registered x-ray powder-diffraction diagrams of the U. S. B. S. dolomite No. 88. Upper, after 3 hrs., middle, after 50 hrs., and lower, after 228 hrs.

Miller indices will be used in the following discussion to refer only to the true rhombohedral cell. Analogous cubic directions can then be referred to by name. Table 2 presents the various index correlations for the commoner dolomite forms.

Translation gliding of dolomite with $T\{111\}$, $t[10\bar{1}]$ was produced experimentally by Johnsen (7), and twin gliding on $\{110\}$, probably along the short diagonals of the cleavage rhomb, is discussed by Fairbairn and Hawkes (4). Both of these are octahedral glides along dodecahedral poles in the cubic system. The familiar pressure twins of calcite across (332) are not known in dolomite. This is the "forbidden" dodecahedral translation along a cube pole. It occurs in calcite only as a twin glide, not as a full translation.

Figures 4, 5, and 6 are projections of the dolomite structure onto $(1\bar{1}0)$ arranged as discussed by Fairbairn and Hawkes. Figure 4 is a projection of the aspect a calcite pressure twin would assume in dolomite if it did occur.

TABLE 2. SPECIMEN INDEX FORM CORRELATIONS FOR VARIOUS DOLOMITE REFERENCE AXES

Rhombohedral unit cell	Cleavage rhomb.*	Crystallographers hexagonal*	Hexagonal structure cell $a=4.8$ Å $c=16$ Å	Edge-centered rhomb.	Face
100	$[3\bar{1}\bar{1}]$	$[40\bar{4}1]$	$10\bar{1}1$	$\bar{1}11$	M
110	$11\bar{1}$	$[02\bar{2}1]$	$01\bar{1}2$	002	f
211	200	$10\bar{1}1$	$10\bar{1}4$	022	r
222	111	[0001]	0006	222	c
221	$[33\bar{1}]$	$[04\bar{4}5]$	$01\bar{1}5$	113	l'
$10\bar{1}$	$20\bar{2}$	$11\bar{2}0$	$11\bar{2}0$	$\bar{2}02$	a
210	$[51\bar{3}]$	$[44\bar{8}3]$	$11\bar{2}3$	$\bar{1}13$	α
$11\bar{1}$	$[33\bar{5}]$	$[08\bar{8}1]$	$02\bar{2}1$	$\bar{1}\bar{1}3$	d
322	[511]	$[40\bar{4}7]$	$10\bar{1}7$	133	
332	220	$01\bar{1}2$	$01\bar{1}8$	224	e
321	$31\bar{1}$	$[22\bar{4}3]$	$11\bar{2}6$	024	
$20\bar{1}$	$[71\bar{5}]$	$[8\cdot4\cdot\bar{1}\bar{2}\cdot1]$	$21\bar{3}1$	$\bar{3}13$	k
$21\bar{1}$	$31\bar{3}$	$[24\bar{6}1]$	$12\bar{3}2$	$\bar{2}04$	
310	$40\bar{2}$	$21\bar{3}1$	$21\bar{3}4$	$\bar{2}24$	v
$2\bar{1}\bar{1}$	$4\bar{2}\bar{2}$	$30\bar{3}0$	$30\bar{3}0$	$\bar{4}22$	m

* Brackets denote that reflections appear for fractional orders under these conventions.

When calcite is pressure-twinned the ions of each successive (332) level are displaced along a "cube" pole to the alternative equivalent position, which represents the exchange of the long for the short diagonal of the cleavage rhomb, and CO_3 ions rotate according to the steric requirements. Each successive level makes this exchange as the twin boundary

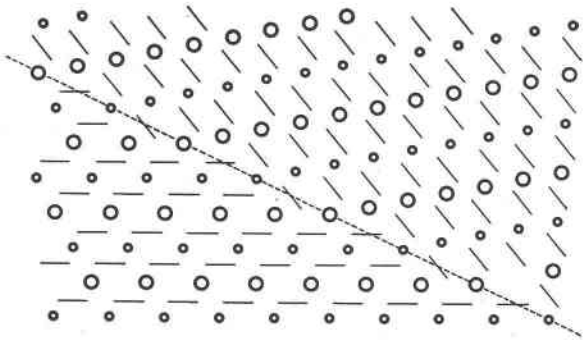

FIG. 4. A $(1\bar{1}0)$ projection of the aspects which dolomite would exhibit at the twin boundary if the familiar calcite type (332) twin were produceable by pressure. Large circles represent Ca, small circles, mg, and lines, CO_3.

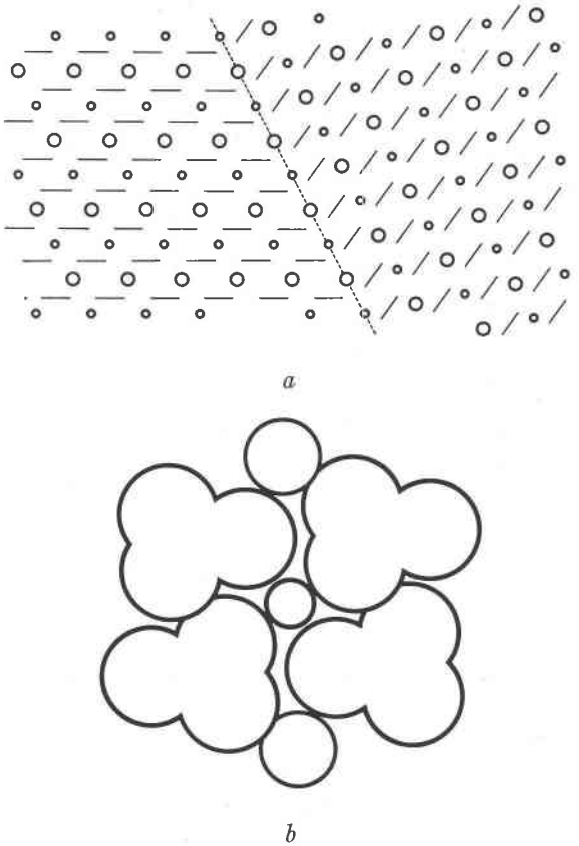

FIG. 5. A $(1\bar{1}0)$ projection (*a*) of the twin boundary of dolomite for the (110) pressure twin, illustrating the identity of the original and synthesized members. The supplemental sketch (*b*) is a view of the packing arrangement in a cleavage rhomb face.

progresses through successive 332 levels, but no level glides beyond the like-ion barrier of the "cube" pole glide. The result is that the (222) and one of the (110) directions interchange, and inasmuch as the projection of the structure upon each is a simple alternation of Ca and CO_3 ions, no drastic rearrangement has been required.

As is seen in figure 4, the application of the identical mechanism to dolomite fails as a physical possibility because of the unequal Ca and Mg ion sizes and dispositions. Projected ion sequences along [111] and [110] are, respectively, Ca, CO_3, Mg, CO_3, etc., and Ca+Mg, $2CO_3$, Ca+Mg, $2CO_3$, etc., which are not interchangeable. A pressure twin of composition face (332) would require a complete redistribution of the positive ions.

Figure 5 illustrates the apparent mechanism of the formation of the lamellar dolomite twins across (110). Not apparent in this projection, but clear in three dimensions and in the supplemental sketch, is the fact that alternating CO_3 levels as projected onto [111] have oxygen atoms pointed alternately toward and away from the possible short diagonal glide lines. Thus in gliding, a protruding oxygen atom can pass a Mg position with less friction than it can a Ca position, and a mechanism is set up to favor translations of one level only. It is seen that such unit glides (modified only by a small twin glide) along succeeding short diagonals for each successive (110) level redistribute the positive ions into dolomite successions in the synthesized twin, and simple rotation of the affected carbonate groups builds a twinned lamella. It seems reasonable that the natural twinned lamellae are so produced.

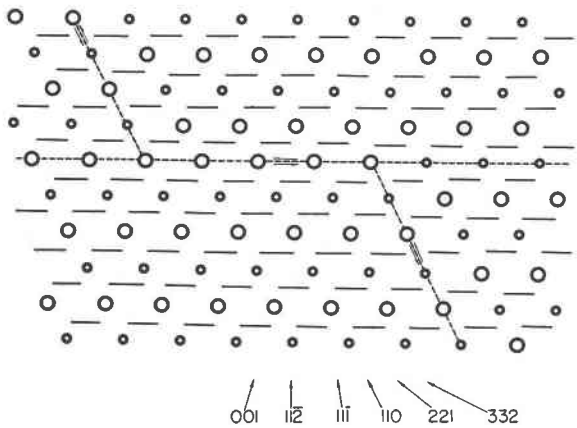

FIG. 6. A (1$\bar{1}$0) projection of a detail of a dolomite structure which has been subjected successively to a unit glide on (110) and a glide of several units on (222).

The probable mechanism of the deformation in the grinding experiments described earlier is illustrated in figure 6. The section depicts a detail of the crossing of a unit glide on (110) by a longer glide on (111). Under the varying directions and magnitudes of the loads impressed in grinding, this detail must be reproduced an enormous number of times in the reduction of natural texture dolomite rocks to impalpable powders. Each such intersection of glides produces a nucleus within the dolomite structure in which all neighbors of some carbonate groups are either all Ca or all Mg, and therefore repeated crosses can build up substantial Ca-rich and Mg-rich islands. In the same mechanism the phase relations of positive ions within coherently scattering domains are disrupted. Consequently, the diffraction lines which are peculiar to dolomite, and which

derive their intensity mainly from the difference in scattering power between Ca and Mg, are attenuated. Such lines are thus distinguished from those to which the Ca and Mg make contributions of equal sign, and from those to which the major contributor is oxygen.

Haul and others (5, 6, 10) have recently discussed the thermal decomposition of dolomite and have noted the evidence for an activation energy. In consideration of the observation that calcite and periclase are produced essentially simultaneously, the calcite, at least, being synthesized at orientations controlled by the original dolomite structure, it seems reasonable to assume that the activation energy is associated with interdiffusion of positive ions to produce Ca-rich and Mg-rich localities. This kind of sorting having already been accomplished mechanically by grinding, in the case of the vigorously ground material above, thermal decomposition of this powder proceeds at a notably reduced temperature, more comparable with that at which magnesite itself decomposes.

The authors wish to acknowledge gratefully the help of Dr. Richards A. Rowland and Dr. H. T. Byck in editing this paper and the cooperation of the Koninklijke/Shell-Laboratorium, Amsterdam, which very kindly took the x-ray diffraction patterns shown in figure 3.

References

1. Bragg, W. L., Atomic Structure of Minerals: Cornell University Press, 281 pp. (1937).
2. Buerger, M. J., Translation gliding in crystals of the NaCl structural type: *Am. Mineral.*, **15,** 180, 226 (1930).
3. Elliott, Norman, A redetermination of the carbon-oxygen distance in calcite and the nitrogen-oxygen distance in sodium nitrate: *Jour. Am. Chem. Soc.*, **59,** 1380–1382 (1937).
4. Fairbairn, H. W., and Hawkes, H. E., Jr., Dolomite orientation in deformed rock: *Am. Jour. Sci.*, **239,** 617–632 (1941).
5. Haul, R. A. W., and Heystek, H., Differential thermal analysis of the dolomite decomposition: *Am. Mineral.*, **37,** 166–180 (1952).
6. Haul, R. A. W., and Heystek, H., Differentielle thermische Analyse der Dolomitzersetzung: *Die Naturwissenschaften*, **38,** 283–284 (1951).
7. Johnsen, A. Biegungen und Translationen: *Jahrbuch Min.*, **II,** 133 (1902).
8. Pauling, L., and Sherman J., Screening constants for many-electron atoms. The calculation and interpretation of x-ray term values and the calculation of atomic scattering factors: *Zeit. Krist.*, **81,** 1–29 (1932).
9. Rowland, Richards A., and Lewis, Donald R., Furnace atmosphere control in differential thermal analysis: *Am. Mineral.*, **36,** 80–91 (1951).
10. Wilsdorf, H. G. F., and Haul, R. A. W., X-ray study of the thermal decomposition of dolomite: *Nature*, **167,** 945–946 (1951).

Manuscript received June 6, 1952.